Control of equatorial ionospheric morphology by atmospheric tides

T. J. Immel,[1] E. Sagawa,[2] S. L. England,[1] S. B. Henderson,[3] M. E. Hagan,[4] S. B. Mende,[1] H. U. Frey,[1] C. M. Swenson,[3] and L. J. Paxton[5]

Received 27 February 2005; revised 20 April 2006; accepted 21 June 2006; published 10 August 2006.

[1] A newly discovered 1000-km scale longitudinal variation in ionospheric densities is an unexpected and heretofore unexplained phenomenon. Here we show that ionospheric densities vary with the strength of nonmigrating, diurnal atmospheric tides that are, in turn, driven mainly by weather in the tropics. A strong connection between tropospheric and ionospheric conditions is unexpected, as these upward propagating tides are damped far below the peak in ionospheric density. The observations can be explained by consideration of the dynamo interaction of the tides with the lower ionosphere (E-layer) in daytime. The influence of persistent tropical rainstorms is therefore an important new consideration for space weather. **Citation:** Immel, T. J., E. Sagawa, S. L. England, S. B. Henderson, M. E. Hagan, S. B. Mende, H. U. Frey, C. M. Swenson, and L. J. Paxton (2006), Control of equatorial ionospheric morphology by atmospheric tides, *Geophys. Res. Lett.*, *33*, L15108, doi:10.1029/2006GL026161.

[2] The ionosphere is the region of highest plasma density in Earth's space environment. It is a dynamic environment supporting a host of plasma instability processes, with important implications for global communications and geo-location applications. Produced by the ionization of the neutral atmosphere by solar x-ray and UV radiation, the uppermost ionospheric layer has the highest plasma density with a peak around 350–400 km altitude and primarily consists of O^+ ions. This is called the F-layer and it is considered to be a collisionless environment such that the charged particles interact only weakly with the neutral atmosphere, lingering long after sunset. The E-layer is composed of molecular ions and is located between ~100–150 km where collisions between ions and neutrals are much more frequent, with the result that the layer recombines and is reduced in density a hundredfold soon after sunset [*Rees*, 1989; *Heelis*, 2004]. The respective altitude regimes of these two layers are commonly called the E- and F-regions.

[3] The ionosphere glows as O^+ ions recombine to an excited state of atomic oxygen (O I) at a rate proportional to the product of the electron and O+ densities, Figure 1 shows an image of the Earth obtained at the far-ultraviolet (FUV) 135.6-nm wavelength, produced in the ^5S-^3P transition of O I. The ionosphere is significantly structured, with dense bands of plasma at low latitudes straddling the magnetic equator of Earth. This is the equatorial ionospheric anomaly (EIA) [*Namba and Maeda*, 1939; *Appleton*, 1946]. Prominent from daytime to evening sectors, these bands are a result of the uplift of ionospheric plasma at the equator to altitudes >800 km and the subsequent diffusion down magnetic field lines. The uplifting process is driven by eastward dynamo electric fields generated by the interaction of neutral winds in the lower thermosphere with the daytime ionospheric E-layer. Figure 2 describes this process. Any phenomenon that can interfere with this process, particularly by changing the daytime electric field (Figure 2 highlight (1)), can therefore affect the growth of the EIA.

[4] Active atmospheric phenomena in this region include atmospheric thermal tides, planetary-scale internal waves driven by the diurnal heating cycle [*Chapman and Lindzen*, 1970]. Conversion of solar radiation to heat directly energizes many tidal modes throughout the atmosphere, but the largest tides at E-region altitudes originate in the atmosphere below, rising in height and magnitude to dominate the weaker, locally driven tidal wind structures [*Williams and Avery*, 1996; *Miyahara and Miyoshi*, 1997; *Hagan and Forbes*, 2003; *Forbes et al.*, 2003]. Dynamical atmospheric simulations indicate the importance of tides in determining conditions in this region of the atmosphere [*Akmaev and Shved*, 1980; *Roble and Shepherd*, 1997]. Recent simulations performed to study the effect of upward-propagating tidal energy in a global circulation model showed that several of the major diurnal tidal modes have a significant influence on the vertical plasma drifts in the F-region during the daytime [*Millward et al.*, 2001]. Until now, no observations supporting this work have ever been made.

[5] Because the upward-propagating tides are heavily damped at and above the E-layer, one may not initially expect lower-atmospheric tides to affect the properties of the F-layer directly. However, upward-propagating tides should modulate the E-layer dynamo electric fields produced as winds push plasma perpendicular to the magnetic field. These electric fields largely control the daytime development of the F-layer. In a related manner, day-to-day variability in the ionospheric electric current system has been attributed to variations in tidal strength [*Stening*, 1975]. As heat exchange in the lower atmosphere and radiative absorption throughout the atmosphere generate a large number of tides with common frequencies but different propagation characteristics, longitudinal variations in the combined tidal strength exist at E-layer altitudes [*Hagan and Forbes*, 2002]. Therefore, one may postulate that these could induce a longitudinal variation in the E-layer dynamo and hence in

[1]Space Sciences Laboratory, University of California, Berkeley, California, USA.
[2]National Institute of Information and Communications Technology, Tokyo, Japan.
[3]Department of Electrical and Computer Engineering, Utah State University, Logan, Utah, USA.
[4]High Altitude Observatory, National Center for Atmospheric Research, Boulder, Colorado, USA.
[5]Johns Hopkins University Applied Physics Laboratory, Laurel, Maryland, USA.

0094-8276/06/2006GL026161

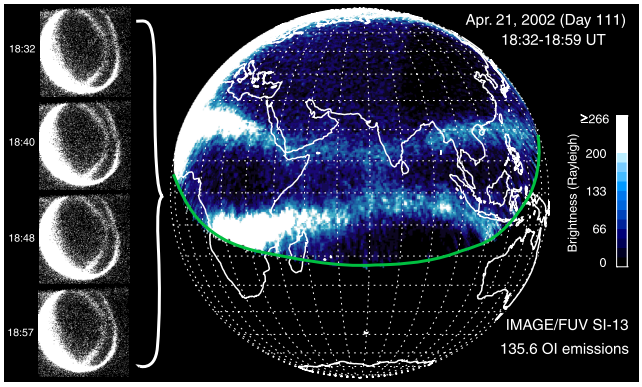

Figure 1. Projection of ionospheric ultraviolet emissions measured by IMAGE-FUV onto a grid of geographic coordinates. 14 5-second images obtained over 28 minutes of time are combined to produce an average emission map. Selected raw FUV images are shown to the left, showing the bright airglow on the dayside and the glowing ionospheric anomalies stretched across the night. Both the northern and southern equatorial ionospheric anomalies are visible here, though the southern anomaly is near the edge of the field-of-view. The green line in the mapped image indicates the edge of viewable locations on Earth from the satellite's point-of-view.

the development of the dayside F-layer. To date, investigations of ionospheric structure in the F-layer and above have either found no evidence of such a longitudinal variation, or found a variation that would be inconsistent with tidal forcing [*Coley et al.*, 1990; *Fejer et al.*, 1995]. Recent studies using space-based magnetometers [*Ivers et al.*, 2003; *Lühr et al.*, 2004] or ionospheric density measurements [*Vladimer et al.*, 1999] have found some new indications of longitudinal ionospheric structure, but those studies discussed no causal mechanisms. A connection to tides has been recently suggested [*Jadhav et al.*, 2002; *Sagawa et al.*, 2005], and this work is undertaken to test these hypotheses of tidal influence.

[6] The IMAGE satellite can observe the nighttime 135.6–nm emissions of the EIA for up to six hours of each 14-hour orbit, allowing the temporal and spatial evolution of the plasma to be monitored [cf. *Immel et al.*, 2003, *Lin et al.*, 2005]. The present study uses the particularly clear observations that IMAGE made in March and April 2002, such as the example of Figure 1, to examine the large-scale morphology of the EIA around equinox. We collected and averaged all of the nightside FUV observations between March 20 and April 20 as a function of local time, magnetic latitude and longitude. Then, the mean coefficients of a Gaussian fit to the latitudinal distribution of emissions are determined in every local time and longitude sector to determine the mean morphology of the ionosphere. The resultant image shown in Figure 3 presents a reconstruction of the ionospheric emissions from those coefficients for the 20:00 local time sector, showing the mean ionospheric state. A greater mean separation of the EIA peaks is evident at four locations around the planet: South America, Africa, Southeast Asia, and the central Pacific. The repeated separation and rapprochement of the EIA peaks in Figure 3 was identified by *Sagawa et al.* [2005], who noted that this structure cannot be explained by any simple interaction of the known electric and magnetic fields that combine to produce the EIA. We have reproduced the southern band by assuming conjugacy and mapping the northern band across the magnetic equator, which is valid for equinox. Some asymmetry may be expected where the magnetic equator depart significantly from the geographic equator.

[7] Overlaid on this image are contours of the equinoctial amplitude of the diurnal temperature variation at 115 km determined from the Global Scale Wave Model (GSWM) [*Hagan et al.*, 2001; *Hagan and Forbes*, 2002, 2003; *Forbes et al.*, 2003]. Equinoctial model outputs are selected for best comparison to the March–April FUV data. Peaks in the temperature amplitude along the equator indicate areas where the major components of the diurnal tide combine most effectively to alter winds and temperatures at the given altitude. A remarkable correspondence between the peaks in tidal strength and the maxima in the separation of the peaks is evident. The relationship is notable in comparisons with the brightness of the EIA as well. Conversely, the anomalies draw much closer together and are generally fainter where the tidal forcing is weakest, particularly over the Indian Ocean.

[8] A closer investigation of the tides and the ionospheric distribution further demonstrates the correspondence between the tidal temperatures in the E-region and both the latitude and brightness of the anomaly. Figure 4a shows this by comparing diurnal tidal temperature amplitudes at 115-km altitude along the equator (dashed blue line) and latitude of peak brightness in the northern anomaly (black line). The correspondence between the parameters is evident, with 4 matching peaks and one additional peak in the FUV measurements at the location of a tidal temperature minimum at longitudes of ~330°. We discuss this single discrepancy later in the report. Also shown here is the latitude of the northern anomaly from a new model of the

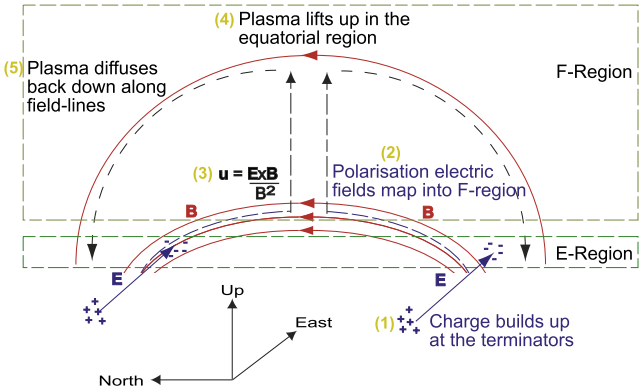

Figure 2. Diagram describing the development of the equatorial ionospheric anomaly, the magnetic and electric fields that combine to produce it. (1) The E-region dynamo, driven by neutral wind-E-layer interaction, produces an eastward electric field across the dayside. (2) These fields are transmitted upward along magnetic field lines into the F-region, causing the plasma to $\mathbf{E} \times \mathbf{B}$ drift upward (3, 4) at the magnetic equator. (5) Through diffusion and gravitational sedimentation, the upward lifted plasma settles along the magnetic field to locations north and south of the equator.

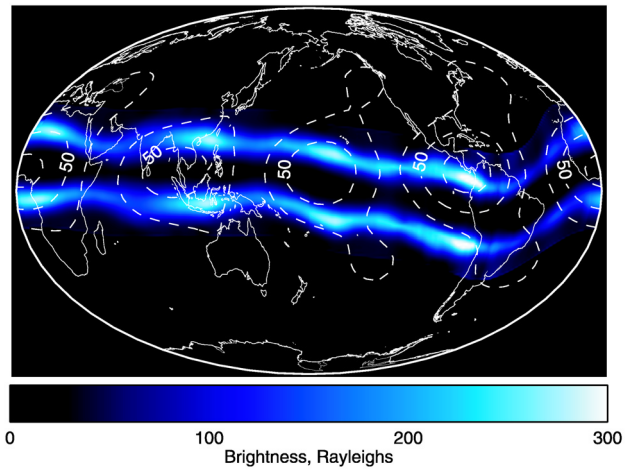

Figure 3. Reconstruction of nighttime ionospheric emissions from 30 days (March 20–April 20) of observations with the IMAGE-FUV imager. The average location and brightness of the equatorial ionospheric anomaly stand out in this presentation. Due to the poor sampling of emissions from the southern anomaly, it is represented here with a mirror image of the northern anomaly across the magnetic equator. This image is representative of the local ionospheric properties at 20:00 LT. Overlaid on this figure with white dashed contours is the amplitude of the diurnal temperature variation at 115 km due to upward-propagating lower atmospheric tides, as reported by the GSWM.

EIA constructed using FUV data from the NASA TIMED mission [*Henderson et al.*, 2005a, 2005b]. The IMAGE and TIMED measurements of the latitude of the EIA agree remarkably well, and both match the temperature peaks from the GSWM.

[9] Just as the latitude of the anomaly can be used as an indication of the strength of the processes that helped form it during the day, the density of the anomaly can also indicate the strength of the formation process. The brightness of the northern anomaly is shown in Figure 4b, alongside the tidal temperature amplitudes in a similar format similar as Figure 4a. Figure 4b demonstrates a clear relationship between the tidal strength and density of the anomaly. The brightness peaks nearly coincide with the four tidal amplitude peaks. The TIMED model of ionospheric emission brightness is also shown, again agreeing very well with the IMAGE data. The longitudinal offset between the FUV and tidal peaks is more pronounced than in Figure 4a, though also present in that previous plot.

[10] The temperature amplitudes shown in Figure 4a indicate the longitudes at which the combined diurnal tidal oscillations maximize. According to the GSWM, the phase of this oscillation is such that the meridional wind component in the vicinity of the E-layer peak maximizes close to local noon, with winds blowing away from the temperature maximum at the equator at that time. The density of the E-layer, and the degree of ion-neutral coupling in the E-region, also reaches its peak at noon. The upward-propagating tides therefore enhance the regular noon-time E-region dynamo wind that is also directed away from the equator at noon, which supports the growth of the daytime low-latitude F-layer. This reinforcement of the background dynamo winds is concentrated in four peaks around the globe where the tides are greatest. The interaction will enhance the dynamo electric field in these four regions, resulting in the global-scale variation in the morphology of the EIA that we observe.

[11] Aside from the dayside dynamo electric field, the most important low-latitude ionospheric phenomenon is the pre-reversal enhancement (PRE) in the uplifting, eastward electric field that occurs near sunset. Using a coupled atmospheric-ionospheric model, *Millward et al.* [2001] showed that lower thermospheric tides can strongly modulate the dayside dynamo electric field while having practically no effect on the PRE. This is due in part to the phase of the tidal forcing approaching zero at the terminators. Though this may be reconsidered for the solar-maximum conditions present in 2002, it is likely that the PRE is not the mediator of energy transfer from the lower atmosphere

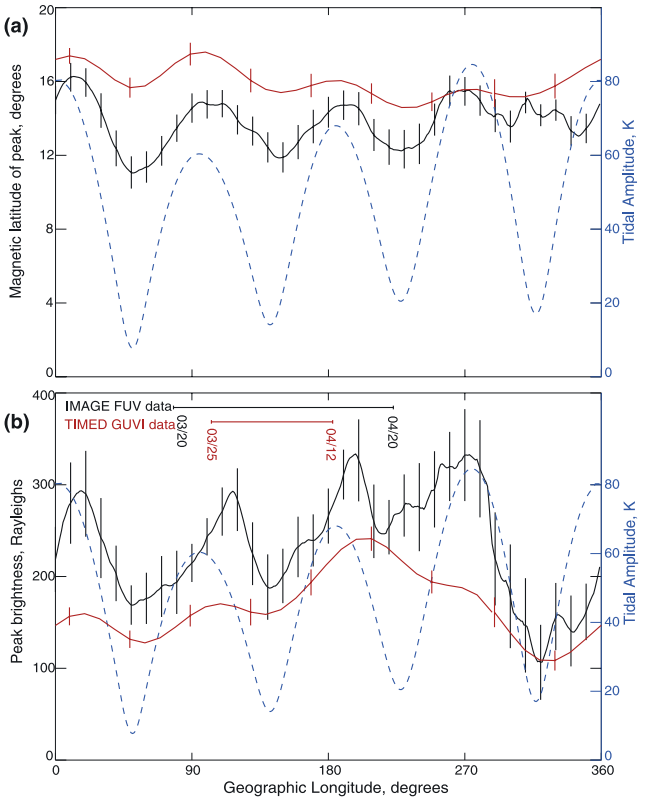

Figure 4. Figure 4a shows the average latitude of the peak brightness (vs. longitude) of the EIA determined from IMAGE FUV images of the 135.6-nm recombination airglow emissions (black line) in the 20:30-22:00 LT sector. The red line shows the same parameter from an ionospheric model developed using FUV observations from the TIMED satellite. The blue dashed line shows the amplitude of the temperature variation driven by the diurnal tide at 115 km, as reported by the GSWM. The 2–3° overall latitudinal offset between the IMAGE data and TIMED model are likely due to uncertainty in the exact height of the F-layer (assumed for this work to be 400 km), which weighs on the remote IMAGE observations. Figure 4b shows the brightness of the EIA (vs. longitude) from IMAGE and TIMED in a format similar to Figure 4a. The data used in the TIMED model are entirely within the period of IMAGE observations.

to the ionosphere, but rather (possibly) an amplifier of the wave-4 zonal morphology as the tide-modified ionosphere rotates to the nightside.

[12] It is clear that coupling between the lower and upper regions of the atmosphere must be addressed in terms of the momentum carried by the atmospheric tides. Although the upward-propagating tidal momentum is heavily damped at upper E-region altitudes, it is now apparent that the polarization electric fields the tides produce are transmitted upward along the magnetic field into the F-region with significant results. We find that recent simulations of tidal effects on upper atmospheric electric fields were accurate in their predictions of significant modification of the dynamo electric fields by upward-propagating tides [*Millward et al.*, 2001]. The good correspondence of the tidal parameters from the GSWM with two separate FUV ionospheric imaging analyses of the structure of the EIA strongly supports our conclusion that the longitudinal variability in the EIA results from lower-atmospheric tidal forcing of the upper atmosphere. No other known terrestrial phenomenon or combination thereof could induce this type of variability in the F-region, and the close correspondence of peak densities and latitudinal separation of the EIA bands indicates a modulation of ionospheric growth. This growth is driven on the dayside by the E-region dynamo electric field (see Figure 1), the very electric field that we believe is modified by the longitudinal structure in the tidal winds.

[13] The four-peaked longitudinal signature is unique to Earth, with its particular distribution of landmasses and associated meteorological forcing. It is found at equinox times, when the meridional component of E-region neutral winds at low latitudes is not dominated by inter-hemispheric flows. We expect that the troposphere-ionosphere coupling will be greatest at the peak of the solar-cycle when E-region densities are highest. Questions remain, however, about the relative importance of the diurnal and semi-diurnal tides, the seasonal variation of the tidal effects, magnetic conjugacy, and the large-scale impulsive effects of prodigious producers of wave energy such as tropical cyclones. Answering these questions will require significant cooperation between scientific communities that often specialize in particular altitude regions of the atmosphere (e.g., troposphere vs. thermosphere). Ionospheric studies from ground and space will need to be undertaken using this new knowledge as a basis.

[14] **Acknowledgments.** IMAGE FUV analysis is supported by NASA through Southwest Research Institute subcontract number 83820 at the University of California, Berkeley, contract NAS5-96020. Additional SI-13 analyses are supported through NASA SEC Guest Investigator Grant NNG04GH05G also at the University of California, Berkeley.

References

Akmaev, R. A., and G. M. Shved (1980), Modelling of the composition of the lower thermosphere taking account of the dynamics with applications to tidal variations of the forbidden 5577 Å airglow, *J. Atmos. Terr. Phys.*, *42*, 705–716.

Appleton, E. V. (1946), Two anomalies in the ionosphere, *Nature*, *157*, 691.

Chapman, S., and R. S. Lindzen (1970), *Atmospheric Tides*, Springer, New York.

Coley, W. R., J. P. McClure, and W. B. Hanson (1990), Equatorial fountain effect and dynamo drift signatures from AE-E observations, *J. Geophys. Res.*, *95*, 21,285–21,290.

Fejer, B. G., E. R. de Paula, R. A. Heelis, and W. B. Hanson (1995), Global equatorial ionospheric vertical plasma drifts measured by the AE-E satellite, *J. Geophys. Res.*, *100*, 5769–5776.

Forbes, J. M., M. E. Hagan, S. Miyahara, Y. Miyoshi, and X. Zhang (2003), Diurnal nonmigrating tides in the tropical lower thermosphere, *Earth Planets Space*, *55*, 419–426.

Hagan, M. E., and J. M. Forbes (2002), Migrating and nonmigrating diurnal tides in the middle and upper atmosphere excited by tropospheric latent heat release, *J. Geophys. Res.*, *107*(D24), 4754, doi:10.1029/2001JD001236.

Hagan, M. E., and J. M. Forbes (2003), Migrating and nonmigrating semidiurnal tides in the upper atmosphere excited by tropospheric latent heat release, *J. Geophys. Res.*, *108*(A2), 1062, doi:10.1029/2002JA009466.

Hagan, M. E., R. G. Roble, and J. Hackney (2001), Migrating thermospheric tides, *J. Geophys. Res.*, *106*, 12,739–12,752.

Heelis, R. A. (2004), Electrodynamics in the low and middle latitude ionosphere: A tutorial, *J. Atmos. Sol. Terr. Phys.*, *66*, 825–838.

Henderson, S. B., C. M. Swenson, J. H. Gunther, A. B. Christensen, and L. J. Paxton (2005a), Method for characterization of the equatorial anomaly using image subspace analysis of Global Ultraviolet Imager data, *J. Geophys. Res.*, *110*, A08308, doi:10.1029/2004JA010830.

Henderson, S. B., C. M. Swenson, A. B. Christensen, and L. J. Paxton (2005b), Morphology of the equatorial anomaly and equatorial plasma bubbles using image subspace analysis of GUVI data, *J. Geophys. Res.*, *110*, A11306, doi:10.1029/2005JA011080.

Immel, T. J., S. B. Mende, H. U. Frey, L. M. Peticolas, and E. Sagawa (2003), Determination of low latitude plasma drift speeds from FUV images, *Geophys. Res. Lett.*, *30*(18), 1945, doi:10.1029/2003GL017573.

Ivers, D., R. Stenning, J. Turner, and D. Winch (2003), Equatorial electrojet from Ørsted scalar magnetic field observations, *J. Geophys. Res.*, *108*(A2), 1061, doi:10.1029/2002JA009310.

Jadhav, G., M. Rajaram, and R. Rajaram (2002), A detailed study of equatorial electrojet phenomenon using Ørsted satellite observations, *J. Geophys. Res.*, *107*(A8), 1175, doi:10.1029/2001JA000183.

Lin, C. S., T. J. Immel, H.-C. Yeh, S. B. Mende, and J. L. Burch (2005), Simultaneous observations of equatorial plasma depletion by IMAGE and ROCSAT-1 satellites, *J. Geophys. Res.*, *110*, A06304, doi:10.1029/2004JA010774.

Lühr, H., S. Maus, and M. Rother (2004), Noon-time equatorial electrojet: Its spatial features as determined by the CHAMP satellite, *J. Geophys. Res.*, *109*, A01306, doi:10.1029/2002JA009656.

Millward, G. H., et al. (2001), An investigation into the influence of tidal forcing on *F* region equatorial vertical ion drift using a global ionosphere-thermosphere model with coupled electrodynamics, *J. Geophys. Res.*, *106*, 24,733–24,744.

Miyahara, S., and Y. Miyoshi (1997), Migrating and non-migrating atmospheric tides simulated by a middle atmosphere general circulation model, *Adv. Space Res.*, *20*(6), 1201–1207.

Namba, S., and K.-I. Maeda (1939), *Radio Wave Propagation*, 86 pp., Corona, Tokyo.

Rees, M. H. (1989), *Physics and Chemistry of the Upper Atmosphere*, Cambridge Univ. Press, New York.

Roble, R. G., and G. G. Shepherd (1997), An analysis of wind imaging interferometer observations of $O(^1S)$ equatorial emission rates using the thermosphere-ionosphere-mesosphere-electrodynamics general circulation model, *J. Geophys Res.*, *102*, 2467–2474.

Sagawa, E., T. J. Immel, H. U. Frey, and S. B. Mende (2005), Longitudinal structure of the equatorial anomaly in the nighttime ionosphere observed by IMAGE/FUV, *J. Geophys. Res.*, *110*, A11302, doi:10.1029/2004JA010848.

Stening, R. J. (1975), Problems of identifying lunar geomagnetic effects at Huancayo, *J. Geomagn. Geoelectr.*, *27*, 409–424.

Vladimer, J. A., P. Jastrezebski, M. C. Lee, P. H. Doherty, D. T. Decker, and D. N. Anderson (1999), Longitude structure of ionospheric total electron content at low latitudes measured by the TOPEX/Poseidon satellite, *Radio Sci.*, *34*(5), 1239–1260.

Williams, C. R., and S. K. Avery (1996), Non-migrating diurnal tides forced by deep convective clouds, *J. Geophys. Res.*, *101*, 4079–4091.

S. L. England, H. U. Frey, T. J. Immel, and S. B. Mende, Space Sciences Laboratory, University of California, Berkeley, CA 94720-7450, USA. (immel@ssl.berkeley.edu)

M. E. Hagan, High Altitude Observatory, NCAR, P.O. 3000, Boulder, CO 80307, USA.

S. B. Henderson and C. M. Swenson, Department of Electrical and Computer Engineering, Utah State University, Logan, UT 84322, USA.

L. J. Paxton, Johns Hopkins University Applied Physics Laboratory, Laurel, MD 20723, USA.

E. Sagawa, National Institute of Information and Communications Technology, 4-2-1 Nukui-Kitamachi, Koganei, Tokyo 184-9795, Japan.